ACS APPLIED MATERIALS & INTERFACES

www.acsami.org

Research Article

Electrically Conductive 3D Metal−Organic Framework Featuring π-Acidic Hexaazatriphenylene Hexacarbonitrile Ligands with Anion−π Interaction and Efficient Charge-Transport Capabilities

Ashok Yadav, Dillip K. Panda, Shiyu Zhang, Wei Zhou, and Sourav Saha*

Cite This: https://dx.doi.org/10.1021/acsami.0c12388

Read Online

ACCESS | Metrics & More | Article Recommendations | Supporting Information

ABSTRACT: Semiconducting metal−organic frameworks (MOFs) show great potential to foster myriad advanced electronics and energy technologies, but they must possess adequate charge-carrier concentration and efficient charge-transport pathways in order to display useful electrical conductivity. A new intrinsically conducting 3D framework $[Ag_2(HATHCN)(CF_3SO_3)_2]_n$ was constructed by employing a highly π-acidic 1,4,5,8,9,12-hexaazatriphenylene-2,3,6,7,10,11-hexacarbonitrile (HATHCN) ligand, which assumed a paramagnetic $HATHCN^{\bullet-}$ radical anion character by acquiring electron density from the TfO^- anions involved in the anion−π interaction and facilitated charge movement along the staircase-like $[-Ag^+-HATHCN-]_\infty$ chains having ample $Ag_{4d}{}^+-N_{2p}$ orbital overlap in the valence band region. As a result, the MOF displayed a narrow band gap (1.35 eV) and promising electrical conductivity (7.3×10^{-4} S/cm, 293 K) that ranked very high among those recorded for 3D MOFs. This work presents a new strategy to construct intrinsically conductive 3D frameworks by exploiting the dual metal coordination and anion−π interaction capabilities of a highly π-acidic HATHCN ligand.

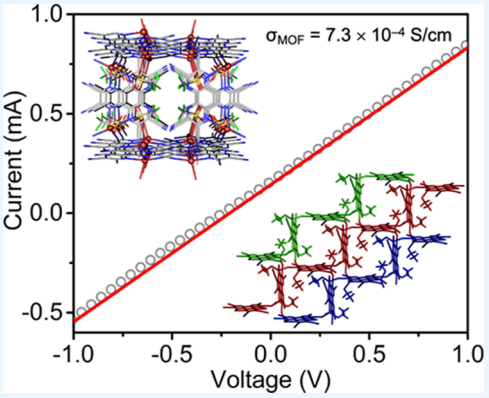

KEYWORDS: *π-acid, anion−π interaction, anion-induced electron transfer, electrical conductivity, metal−organic framework*

INTRODUCTION

The recent progress of electrically conductive metal−organic frameworks (MOFs)[1,2] has unlocked their potential to foster myriad advanced electronics and energy technologies,[3−20] rendering them one of the most coveted functional materials of late. Although these crystalline materials share striking structural similarities with conventional inorganic semiconductors, electrical conductivity (σ) remains one of their most elusive properties because of the lack of adequate charge density and effective charge-transport pathways, the two key conditions of this coveted property.[1,2] While they can be easily furnished with mobile charge carriers (i.e., electrons and holes) by introducing redox-active ligands, metal ions,[21−41] and guests,[42−50] creating efficient charge-transport pathways, especially in 3D frameworks, remains a much greater challenge. Depending on their structures and compositions, charge movement across MOFs occurs predominantly through one of the following routes:[2] metal−ligand bonds,[24−28] π-conjugated ligands,[29−38] π-stacked ligands,[39−43] infiltrated guests,[44−51] and redox hopping,[52−54] and its efficacy has a profound effect on the framework's conductivity. Among these routes, through-bond and resonance charge delocalization are usually more effective than others and consistently lead to higher conductivity than through-space redox hopping.[2] The occurrence of through-bond charge movement requires sufficient metal(d)−ligand(p) orbital overlap, which can be better accomplished with soft N- and S-coordinating ligands and soft transition-metal ions[2,24−28] than with hard carboxylate and oxo-ligands and group I, II, and lanthanide metal ions. Furthermore, fully π-conjugated planar ligands are essential for resonance charge delocalization.[29−38]

While much of the recent attention was focused on developing electrically conducting MOFs based on various electron-rich aromatic ligands, such as hexa-amino/oxo/thia-substituted benzenes and triphenylenes,[34−38] tetrathiafulvalenes,[39−41,49−51] anthracene,[43] and pyrene,[52,53] the π-acidic N-heteroaromatic ligands have been largely overlooked despite their dual capabilities to gain electron density via n-doping and support charge movement through coordination bonds by creating sufficient metal(d)−ligand(p) orbital overlap.[55] Ostensibly absent from the MOFs is a highly π-acidic planar N-heteroaromatic ligand called 1,4,5,8,9,12-hexaazatriphenylene-2,3,6,7,10,11-hexacarbonitrile (HATHCN),[56] which can not only coordinate soft transition-metal ions with its 2,2′-

Received: July 8, 2020
Accepted: August 13, 2020
Published: August 13, 2020

bipyridine-like core N-atoms and terminal CN groups[57−59] but also interact with different anions ranging from highly Lewis basic OH^-, F^-, and CN^- to charge diffuse TfO^-, PF_6^-, and $[M(CN)_x]^{y-}$ (M = Ni^{II}, Pt^{II}, Pd^{II}, Fe^{III}, Co^{III}, Re^{IV}, and W^V) through anion-induced electron transfer and charge transfer (AIET and AICT)[60−65] and anion−π[66] interactions, leading to the formation of $HATHCN^{\bullet-}$ radical anions under certain conditions. Although anion−π interaction and cation recognition capabilities of HATHCN have been exploited separately for anion sensing, light-harvesting, and myriad other purposes,[67−69] they have never been combined to create an intrinsically conductive MOF. Similarly, the AIET interaction has been used only once[54] to convert a naphthalenediimide (NDI)-based insulating MOF ($\sigma \leq 10^{-14}$ S/cm) to a modest semiconductor (10^{-7} S/cm) by doping it with F^-, which generated $NDI^{\bullet-}$ radical anions. However, the NDI-based MOF lacked efficient charge-transport pathways except charge hopping, which led to a modest electrical conductivity even after extensive F^--induced ligand reduction and the formation of large electron density. Furthermore, F^- has a strong affinity for metal ions, which could disrupt MOF structures. Therefore, it may not be employed universally as a sacrificial electron donor. Unlike the less π-acidic NDI ligands, the highly π-acidic HATHCN can engage soft charge-diffuse anions in anion−π, AIET, and AICT interactions,[60−66] which pose little threat to MOF structures. In addition, the planar HATHCN ligand can also support resonance delocalization, while the NDI ligands cannot because their diimide core and terminal coordinating groups are not coplanar. Therefore, we envisioned that if incorporated into an MOF, the HATHCN ligand could not only acquire electron density from appropriate charge-diffuse anions through anion−π and AIET interactions but also facilitate charge movement through the coordination bonds by providing sufficient metal(d)−ligand(p) orbital overlap and π-conjugation, thereby fulfilling the criteria of electrical conductivity.

Taking advantage of HATHCN's dual cation and anion binding abilities,[56−64] herein, we constructed a new intrinsically conducting 3D MOF $[Ag_2(HATHCN)(CF_3SO_3)_2]_n$ (Figure 1) in which each HATHCN ligand coordinated six Ag^+ cations with four bidentate core N-atoms and four terminal CN groups and also assumed a $HATHCN^{\bullet-}$ radical anion character because of partial electron transfer from the TfO^- anions and metal to ligand charge transfer (MLCT) interaction. The density functional theory (DFT) calculations show a fairly narrow electronic band gap ($E_g \sim 1.35$ eV) of the MOF and significant overlap between Ag^+(4p) and ligand(2p) orbitals in the valence band maximum (VBM) and conduction band minimum (CBM), indicating its ability to support charge movement along the $[-Ag^+-HATHCN-]_\infty$ chains. The *in situ* pressed MOF pellets displayed an average electrical conductivity of ca. $5(2) \times 10^{-4}$ S/cm, with the highest observed value of 7.3×10^{-4} S/cm (293 K), which ranked very high among all existing (sixth out of several dozens) intrinsically conductive 3D frameworks (Table S1). Thus, this work has not only delivered a new intrinsically conductive 3D MOF but, more importantly, demonstrated new strategies to imbue them with mobile charge carriers and facilitate charge movement by leveraging the dual anion recognition and metal coordination capabilities of a highly π-acidic HATHCN ligand.

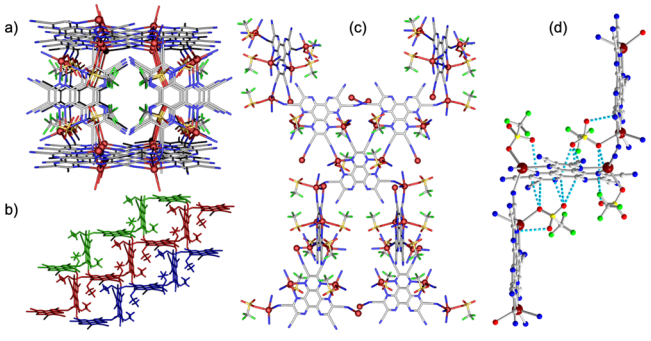

Figure 1. Crystal structure of a $[Ag_2(HATHCN)(CF_3SO_3)_2]_n$ MOF from different angles show the (a) 3D structure, (b) staircase-like $[-Ag^+-HATHCN-]_\infty$ chains that can foster through-bond charge movement, (c) coordination pattern, and (d) anion−π interaction between the Ag^+-bound TfO^- anions and π-acidic HATHCN ligands (Ag^+: metallic magenta balls, C: gray, N: blue, O: red, S: yellow, F: green).

RESULTS AND DISCUSSION

Syntheses and Crystal Structures of HATHCN and $[Ag_2(HATHCN)(CF_3SO_3)_2]_n$ MOFs. HATHCN was synthesized and characterized by following a literature protocol[70] (Supporting Information, Figure S1). Single-crystal X-ray diffraction (SXRD) analysis revealed that (Figure S2) planar HATHCN molecules form offset π-stacks with an interlayer distance of 3.18 Å between overlapping edges.

A room-temperature reaction between HATHCN and AgOTf (1:3 molar ratio) in an undisturbed $MeNO_2$ solution for 48 h afforded orange crystals of $[Ag_2(HATHCN)(CF_3SO_3)_2]_n$ MOF. These crystals were washed thoroughly with $MeNO_2$ and dried under vacuum to obtain the bulk material for further studies. The SXRD analysis showed that the 3D framework (Figure 1a−d) has a tetragonal $I\bar{4}2d$ space group and an asymmetric unit comprising 0.5 HATHCN, one Ag^+, one TfO^-, and one disordered $MeNO_2$ molecule. Each pentavalent Ag^+ ion is coordinated to two 2,2′-bipyridine-like core N-atoms of a HATHCN ligand, two CN groups of two other HATHCN ligands, and a TfO^- anion (Figure 1c). Conversely, each HATHCN ligand chelates two Ag^+ ions with two 2,2′-bipyridine-like sites (four core-N atoms) and binds four more Ag^+ ions with four CN groups. Thus, one 2,2′-bipyridyl site and two adjacent CN groups of each ligand remain metal-free, possibly because of steric congestion and diminished binding ability caused by the coordination of six Ag^+ ions. Each HATHCN ligand also interacts with four Ag^+-bound TfO^- anions via anion−π interaction (Figure 1d), as evident from the short $O\cdots\pi_{centroid}$ distances (ca. 3 Å). There is no $\pi-\pi$ interaction between the ligands as the closest distance between two parallel HATHCN ligands is ca. 13 Å and they are separated by TfO^- anions. Notably, the orthogonally oriented HATHCN ligands linked by Ag^+ cations form staircase-like $[-Ag^+-HATHCN-]_\infty$ coordination chains (Figure 1b) that can potentially facilitate charge movement (*vide infra*). The powder X-ray diffraction (PXRD) patterns of as-synthesized and evacuated materials are in good agreement with the simulated pattern (Figure S3), confirming that the bulk material is phase pure and stable under ambient conditions. The Ag^+−HATHCN coordination was also evident from the Fourier transform infrared spectra: the C≡N stretching frequency red-shifted from 2241 cm^{-1} in free HATHCN to 2161 cm^{-1} in the MOF (Figure S4)[58] as Ag^+-coordination weakened the bond. The X-ray photoemission spectroscopy (Figure S5) displayed the characteristic Ag^+, C,

https://dx.doi.org/10.1021/acsami.0c12388
ACS Appl. Mater. Interfaces XXXX, XXX, XXX−XXX

N, O, F, and S peaks in the MOF, while HATHCN displayed C and N peaks.

Thermogravimetric and Porosity Analyses. The pristine MOF lost ca. 10% weight at 120 °C, indicating solvent loss and then maintained a stable plateau until 300 °C (Figure S6). The PLATON/SQUEEZE model was applied to remove the solvent molecules from the crystal structure, revealing the electron count for a solvent-accessible void of 1054 per unit, which corresponded to 16 $MeNO_2$ molecules per unit. The Brunauer–Emmett–Teller surface area (11.42 m^2/g) and pore volume (1.47×10^{-2} cm^3/g) of the evacuated MOF were estimated from N_2 sorption analysis (Figure S7). These values are consistent with a relatively small solvent-accessible volume (18%) estimated by Mercury software (Figure S8) and comparable to that of another intrinsically conductive but nonporous 3D MOF $(Bu_4N)_2$–$Fe_2^{III}(dhbq)_3$ (dhbq = dihydroxybenzoquinone).[32]

Redox and Optical Properties. The electrochemical behaviors of free HATHCN and the MOF were determined from the cyclic voltammetry (CV) experiments (glassy carbon working electrode, Pt counter electrode, Ag/AgCl reference electrode, 0.1 M $Bu_4NPF_6/MeNO_2$ supporting electrolyte). HATHCN underwent a reversible reduction to $HATHCN^{\bullet-}$ radical anion at −0.17 V, while AgOTf displayed only a cathodic peak corresponding to Ag^+ reduction. The MOF paste adhered to a glassy carbon working electrode displayed a cathodic peak at +0.53 V, indicting Ag^+ reduction, followed by a reversible process at ca. −0.19 V, indicating the formation of $HATHCN^{\bullet-}$ radical anions (Figure S9). Interestingly, the first reduction of HATHCN ligands in the MOF occurred at a slightly more negative potential than that of the free ligand. This may apparently seem counterintuitive given that Ag^+ coordination is expected to further diminish its electron density and thereby facilitate its reduction. However, the electron-withdrawing effect of Ag^+ coordination was possibly counterbalanced by anion–π interaction between each HATHCN ligand and four adjacent TfO^- anions (Figure 1c), which ultimately enhanced the electron density of HATHCN ligands, endowing them a partial $HATHCN^{\bullet-}$ radical anion character (*vide infra*). Although charge-diffuse anions such as TfO^- do not usually share their electron density with ordinary π-acids,[60−65] HATHCN is one of the strongest π-acids (LUMO −4.9 eV)[61,65] and the coordination of six Ag^+ ions—two with the N-heteroaromatic core and four more with four terminal CN groups of each ligand—further enhanced its electron-accepting ability[57,58] and lowered the LUMO level, making partial electron/charge transfer from the TfO^- anions to the enhanced π-acidic HATHCN ligands thermodynamically feasible. In addition, the MLCT interaction between Ag^+ and HATHCN could also contribute to the enhanced electron density of the latter.[57,58] Thus, these two cooperative but opposite effects, that is, Ag^+ coordination and the subsequent partial electron/charge transfer from TfO^- anions to HATHCN ligands, ultimately raised the electron density of the ligands in the MOF, making its electrochemical reduction slightly more difficult than that of the free ligands.

This hypothesis was further supported by electron paramagnetic resonance (EPR) analysis (Figure 2a), which confirmed the presence of paramagnetic $HATHCN^{\bullet-}$ radical anions (g = 1.997) inside the pristine MOF. From quantitative EPR analysis, we estimated that the MOF possessed 8.4×10^{16} spins/mg or 3.8×10^{22} spins/mol, which amounted to ca. 0.1 unpaired electron (spin) in each partially reduced HATHCN ligand.[60−64] As all HATHCN ligands in this MOF have the same coordination pattern and interact with the TfO^- anions in a similar fashion, we inferred that each ligand possessed the same number of unpaired electrons, that is, the same $HATHCN^{\bullet-}$ radical anion character, which stemmed from partial electron/charge transfer from the TfO^- anions involved in anion–π interaction and/or Ag^+/HATHCN MLCT interaction.

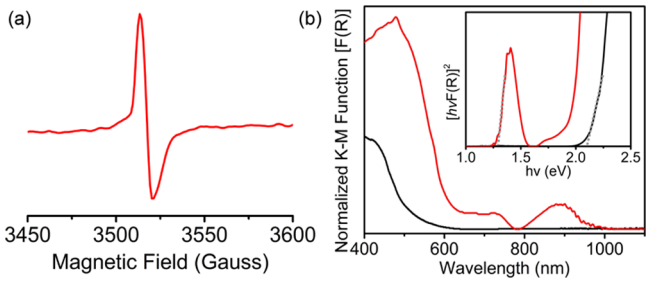

Figure 2. (a) EPR spectrum of the MOF confirms the presence of paramagnetic $HATHCN^{\bullet-}$ radical anions (g = 1.997). (b) Diffuse-reflectance spectra of HATHCN (black trace) and the MOF film (red trace) show the characteristic $HATHCN^{\bullet-}$ radical anion peak in the latter. Inset: The Tauc plots of HATHCN (black trace) and the MOF (red trace) show their optical band gaps for direct transitions.

The partial radical anion nature of HATHCN ligands in the MOF was also evident from its UV–vis–NIR diffuse-reflectance spectrum (Figure 2b). Free HATHCN displayed a characteristic peak at ca. 420 nm, while the MOF displayed an additional peak in the NIR region corresponding to $HATHCN^{\bullet-}$ radical anion absorption.[61] The optical band gaps of free HATHCN ($E_g \sim 2.1$ eV) and the MOF ($E_g \sim 1.3$ eV) were estimated from the corresponding Tauc plots (Figure 2b, inset). The optical band gap of the MOF was in excellent agreement with its electronic band gap estimated by DFT calculations (*vide infra*). The narrower electronic band gap of the MOF than free HATHCN foreshadows a higher electrical conductivity of the former.

While these studies demonstrated the first example of anion–π interaction and partial electron transfer from built-in counteranions to π-acidic HATHCN ligands in an MOF, formal electron transfer from strong Lewis basic anions (OH^-, F^-, CN^-, etc.)[60,61,65] and partial electron/charge transfer from multinuclear $[M(CN)_x]^{y-}$ anions[62−64] to free HATHCN leading to $HATHCN^{\bullet-}$ radical anion formation are well-documented in the literature. In addition, the presence of the $HATHCN^{\bullet-}$ radical anion was also found in discrete trinuclear $[\{Cu(dppX)\}_3(HATHCN)]\cdot Y_2$ complexes[57,58] (dppX = 1,1′-bis(diphenylphosphanyl)- ethylene or ferrocene; Y^- = TfO^- or PF_6^-) consisting of three Cu^+ ions chelated by the 2,2′-bipyridine-like core N-atoms of HATHCN. Although the formation of $HATHCN^{\bullet-}$ in this complex was initially attributed to Cu^+/HATHCN MLCT interaction, in the light of the recent discovery of anion–π, AIET, and AICT interactions,[60−66] it appears that the enhanced π-acidity of HATHCN caused by the coordination of three Cu^+ ions with its core-N atoms triggered partial electron/charge transfer from the TfO^- and PF_6^- counterions located just above and below the HATHCN plane that led to $HATHCN^{\bullet-}$ radical anion formation. In contrast, no $HATHCN^{\bullet-}$ was found in a dimeric $[\{Cu(dpp\text{-}octamethylferrocene)\}_2(HATHCN)_2]\cdot(PF_6)_2$ complex,[58] where the coordination of two Cu^+ ions with two CN groups of each HATHCN ligand did not sufficiently enhance

https://dx.doi.org/10.1021/acsami.0c12388
ACS Appl. Mater. Interfaces XXXX, XXX, XXX−XXX

its π-acidity to activate partial electron transfer from PF_6^- counterions. Thus, the partial $HATHCN^{\bullet-}$ radical anion nature of the ligands in our MOF is fully consistent with those found in the literature.

Electronic Band Structure. To gain deeper insights into the possible charge-transport pathway in a $[Ag_2(HATHCN)(CF_3SO_3)_2]_n$ MOF, we calculated its electronic band structure and density of states (DOS) by DFT calculations. The electronic bands of this MOF are relatively flat (Figure 3, left),

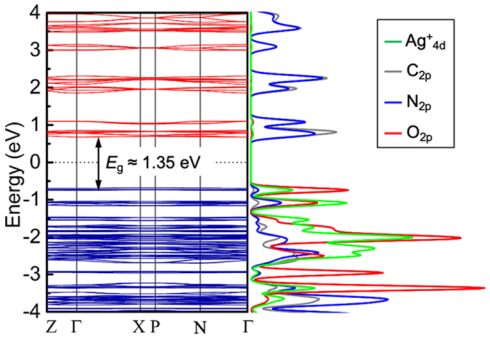

Figure 3. Calculated electronic band structure (left) and corresponding partial DOS (right) of $[Ag_2(HATHCN)(CF_3SO_3)_2]_n$ show its electronic band gap and the contributions of overlapping Ag_{4d}^+ and $ligand_{2p}$ (C, N, and O) orbitals.

which is typical for 3D frameworks with large unit cells; however, it has a fairly narrow electronic band gap of ~1.35 eV, which bodes well for electrical conductivity. The partial DOS diagram (Figure 3, right) shows that the VBM and CBM of the MOF consist of overlapping Ag_{4d}^+ and $ligand_{2p}$ (C, N, and O) orbitals. Specifically, the VBM is largely composed of Ag_{4d}^+, N_{2p}, and O_{2p} orbitals, whereas the CBM is dominated by C_{2p} and N_{2p} orbitals with small contributions from Ag_{4d}^+ and O_{2p} orbitals. The presence of overlapping Ag_{4d}^+ and N_{2p} orbitals in the VBM indicates the hybridization of these two orbitals, foreshadowing the possibility of charge movement along the staircase-like $[-Ag^+-HATHCN-]_\infty$ chains (Figure 1b). Similar metal(d)−ligand(p) orbital overlap in the VBM of other MOFs has also been attributed to their through-bond charge-transport capabilities.[24,25,28,31] Furthermore, the strong contribution of the O_{2p} orbital to the VBM is also consistent with Ag^+-TfO^- coordination and TfO^-/HATHCN anion−π charge transfer interaction, as observed from the crystal structure (Figure 1). Thus, these computational studies provided valuable insights into the electronic property and the potential charge-transport pathway of the MOF.

Electrical Conductivity. Finally, we measured the electrical conductivity of $[Ag_2(HATHCN)(CF_3SO_3)_2]_n$ by a two-probe method using *in situ* pressed pellets sandwiched between two Ag-coated stainless-steel electrodes surrounded by a snugly fit Teflon tube.[51] These MOF pellets displayed a linear current−voltage (I−V) relationship (Figure 4a). The average electrical conductivity of this MOF was ca. $5(2) \times 10^{-4}$ S/cm, with the highest recorded value of 7.3×10^{-4} S/cm (293 K), which surpassed the conductivity of most 3D frameworks (Table S1). The actual electrical conductivity of this MOF is likely much higher because the conductivity values measured by two-probe methods using pressed pellets are usually underestimated by few orders of magnitude because of the contributions of grain boundary and contact resistances that cannot be decoupled.[1,2] The thermal activation energy (E_a

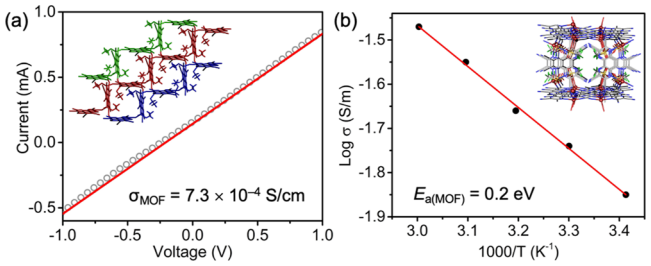

Figure 4. (a) I−V plot of an *in situ* pressed MOF pellet recorded at 293 K used for conductivity measurement. (b) Arrhenius plot of temperature-dependent electrical conductivity of the MOF used for determining E_a.

= 0.2 eV) of the MOF was determined by an Arrhenius plot (Figure 4b) of its temperature-dependent conductivity values (Figure S10). The low activation energy of the MOF is consistent with its relatively high intrinsic electrical conductivity and narrow electronic band gap (~1.35 eV). The PXRD profiles of the MOF recorded before and after electrical measurements were in good agreement (Figure S3), indicating that its structure was largely intact during these processes.

In comparison, the pellets of free HATHCN displayed (Figure S11) a million-fold lower electrical conductivity ($3(1) \times 10^{-10}$ S/cm), even though these molecules are tightly π-stacked in the solid state (Figure S3). Such a striking difference between the conductivities of the MOF and free ligand can be attributed to two factors: (i) the enhanced electron density of HATHCN inside the MOF, that is, a $HATHCN^{\bullet-}$ radical anion character imparted by partial electron transfer from TfO^- anions involved in anion−π interaction and MLCT interaction, and (ii) the possibility of more effective charge transport through the staircase-like $[-Ag-HATHCN-]_\infty$ chains than through the π-stacked free ligands. We believe that both factors likely contributed to the electrical conductivity of this MOF because frameworks with high charge-carrier density but no well-defined charge-transport pathway apart from charge hopping usually display much lower electrical conductivity,[24,53,54] whereas those with efficient charge-transport pathways enjoy higher conductivity.

CONCLUSIONS

In summary, we have constructed a new intrinsically conductive 3D framework by exploiting the dual metal ion coordination and anion−π interaction capabilities of a highly π-acidic HATHCN ligand to fulfill both criteria of electrical conductivity, that is, charge-carrier concentration and facile charge movement. The foregoing results demonstrated that the coordination of each HATHCN ligand with six Ag^+ ions further enhanced its π-acidity, triggering partial electron/charge transfer from the surrounding TfO^- anions involved in anion−π interaction, which rendered it a $HATHCN^{\bullet-}$ radical anion character and enhanced its electron density. At the same time, the overlapping Ag^+ 4d and ligand (C, N, O) 2p orbitals in the VBM and CBM of the MOF created the possibility of charge transport along the staircase-like $[-Ag^+-HATHCN-]_\infty$ chains. As a result, the MOF enjoyed a relatively narrow electronic band gap (~1.3 eV), a low activation energy of charge movement (0.2 eV), and the highest electrical conductivity of 7.3×10^{-4} S/cm (at 293 K), which ranked quite high among those recorded for 3D frameworks. Most importantly, our work demonstrated novel

https://dx.doi.org/10.1021/acsami.0c12388
ACS Appl. Mater. Interfaces XXXX, XXX, XXX−XXX

strategies to enhance the electron density of MOFs through anion−π and AIET interactions and to promote charge movement across frameworks by creating sufficient metal−ligand orbital overlap using a highly π-acidic N-heteroaromatic ligand, which had never been employed in an MOF. We envision that the electron-accepting nature of this MOF could be exploited for optical and chemiresistive sensing of electron-rich species as well as light-harvesting and photovoltaic applications, which are the focus of our ongoing investigations.

■ ASSOCIATED CONTENT

Supporting Information

The Supporting Information is available free of charge at https://pubs.acs.org/doi/10.1021/acsami.0c12388.

Experimental details including materials and methods, synthetic protocols, characterization, device construction, electrical measurement techniques, and additional data (PDF)

Crystallographic data of MOF (CIF)

Crystallographic data of HATHCN (CIF)

Accession Codes

CCDC 1987585 and 1987586 contain supplementary crystallographic data of the MOF and HATHCN ligand, respectively, which can be obtained free of charge from www.ccdc.cam.ac.uk/data_request/cif, data_request@ccdc.cam.ac.uk, or The Cambridge Crystallographic Data Centre, 12 Union Road, Cambridge CB2 1EZ, UK; fax: +44 1223 336033.

■ AUTHOR INFORMATION

Corresponding Author

Sourav Saha − *Department of Chemistry, Clemson University, Clemson, South Carolina 29634, United States;* orcid.org/0000-0001-6610-4820; Email: souravs@clemson.edu

Authors

Ashok Yadav − *Department of Chemistry, Clemson University, Clemson, South Carolina 29634, United States*

Dillip K. Panda − *Department of Chemistry, Clemson University, Clemson, South Carolina 29634, United States*

Shiyu Zhang − *Department of Chemistry, Clemson University, Clemson, South Carolina 29634, United States*

Wei Zhou − *NIST Center for Neutron Research, National Institute of Standards and Technology, Gaithersburg, Maryland 20899, United States;* orcid.org/0000-0002-5461-3617

Complete contact information is available at: https://pubs.acs.org/10.1021/acsami.0c12388

Notes

The authors declare no competing financial interest.

■ ACKNOWLEDGMENTS

This work was supported by the National Science Foundation (award no. DMR-1809092 and CHE-1660329). We acknowledge Drs. Collin McMillen and Kelliann Koehler for their assistance with XRD and XPS analyses, respectively. The XPS facility is supported by the CU Division of Research. DFT calculations were performed in part on the NIST Enki HPC cluster.

■ REFERENCES

(1) Sun, L.; Campbell, M. G.; Dincă, M. Electrically Conductive Porous Metal-Organic Frameworks. *Angew. Chem., Int. Ed.* **2016**, *55*, 3566−3579.

(2) Xie, L. S.; Skorupskii, G.; Dincă, M. Electrically Conductive Metal-Organic Frameworks. *Chem. Rev.* **2020**, *120*, DOI: 10.1021/acs.chemrev.9b00766.

(3) Stavila, V.; Talin, A. A.; Allendorf, M. D. MOF-Based Electronic and Opto-Electronic Devices. *Chem. Soc. Rev.* **2014**, *43*, 5994−6010.

(4) Stassen, I.; Burtch, N.; Talin, A.; Falcaro, P.; Allendorf, M.; Ameloot, R. An updated roadmap for the integration of metal-organic frameworks with electronic devices and chemical sensors. *Chem. Soc. Rev.* **2017**, *46*, 3185−3241.

(5) Wade, C. R.; Li, M.; Dincă, M. Facile Deposition of Multicolored Electrochromic Metal-Organic Framework Thin Films. *Angew. Chem., Int. Ed.* **2013**, *52*, 13377−13381.

(6) AlKaabi, K.; Wade, C. R.; Dincă, M. Transparent-to-Dark Electrochromic Behavior in Naphthalene-Diimide-Based Mesoporous MOF-74 Analogs. *Chem* **2016**, *1*, 264−272.

(7) Dolgopolova, E. A.; Galitskiy, V. A.; Martin, C. R.; Gregory, H. N.; Yarbrough, B. J.; Rice, A. M.; Berseneva, A. A.; Ejegbavwo, O. A.; Stephenson, K. S.; Kittikhunnatham, P.; Karakalos, S. G.; Smith, M. D.; Greytak, A. B.; Garashchuk, S.; Shustova, N. B. Connecting Wires: Photoinduced Electronic Structure Modulation in Metal-Organic Frameworks. *J. Am. Chem. Soc.* **2019**, *141*, 5350−5358.

(8) Wang, H.; Zhu, Q.-L.; Zou, R.; Xu, Q. Metal-Organic Frameworks for Energy Applications. *Chem* **2017**, *2*, 52−80.

(9) Liu, J.; Zhou, W.; Liu, J.; Howard, I.; Kilibarda, G.; Schlabach, S.; Coupry, D.; Addicoat, M.; Yoneda, S.; Tsutsui, Y.; Sakurai, T.; Seki, S.; Wang, Z.; Lindemann, P.; Redel, E.; Heine, T.; Wöll, C. Photoinduced Charge-Carrier Generation in Epitaxial MOF Thin Films: High Efficiency as a Result of an Indirect Electronic Band Gap? *Angew. Chem., Int. Ed.* **2015**, *54*, 7441−7445.

(10) Maza, W. A.; Haring, A. J.; Ahrenholtz, S. R.; Epley, C. C.; Lin, S. Y.; Morris, A. J. Ruthenium(ii)-polypyridyl zirconium(iv) metal-organic frameworks as a new class of sensitized solar cells. *Chem. Sci.* **2016**, *7*, 719−727.

(11) Gordillo, M. A.; Panda, D. K.; Saha, S. Efficient MOF-Sensitized Solar Cells Featuring Solvothermally Grown [100]-Oriented Pillared Porphyrin Framework-11 Films on ZnO/FTO Surfaces. *ACS Appl. Mater. Interfaces* **2018**, *11*, 3196−3206.

(12) Chueh, C.-C.; Chen, C.-I.; Su, Y.-A.; Konnerth, H.; Gu, Y.-J.; Kung, C.-W.; Wu, K. C.-W. Harnessing MOF Materials in Photovoltaic Devices: Recent Advances, Challenges, and Perspectives. *J. Mater. Chem. A* **2019**, *7*, 17079−17095.

(13) Wang, L.; Han, Y.; Feng, X.; Zhou, J.; Qi, P.; Wang, B. Metal-organic frameworks for energy storage: Batteries and supercapacitors. *Coord. Chem. Rev.* **2016**, *307*, 361−381.

(14) Sheberla, D.; Bachman, J. C.; Elias, J. S.; Sun, C.-J.; Shao-Horn, Y.; Dincă, M. Conductive MOF Electrodes for Stable Supercapacitors with High Areal Capacitance. *Nat. Mater.* **2017**, *16*, 220−224.

(15) Li, W.-H.; Ding, K.; Tian, H.-R.; Yao, M.-S.; Nath, B.; Deng, W.-H.; Wang, Y.; Xu, G. Conductive Metal-Organic Framework Nanowire Array Electrodes for High-Performance Solid-State Supercapacitors. *Adv. Funct. Mater.* **2017**, *27*, 1702067.

(16) Zhang, Y.; Riduan, S. N.; Wang, J. Redox Active Metal- and Covalent Organic Frameworks for Energy Storage: Balancing Porosity and Electrical Conductivity. *Chem.—Eur. J.* **2017**, *23*, 16419−16431.

(17) Park, S. S.; Tulchinsky, Y.; Dincă, M. Single-ion Li^+, Na^+, and Mg^{2+} Solid Electrolytes Supported by a Mesoporous Anionic Cu−Azolate Metal−Organic Framework. *J. Am. Chem. Soc.* **2017**, *139*, 13260−13263.

(18) Panda, D. K.; Maity, K.; Palukoshka, A.; Ibrahim, F.; Saha, S. Li^+ Ion-Conducting Sulfonate-Based Neutral Metal−Organic Framework. *ACS Sustainable Chem. Eng.* **2019**, *7*, 4619−4624.

(19) Campbell, M. G.; Sheberla, D.; Liu, S. F.; Swager, T. M.; Dincă, M. Cu_3(hexaiminotriphenylene)$_2$: An Electrically Conductive 2D Metal−Organic Framework for Chemiresistive Sensingr. *Angew. Chem., Int. Ed.* **2015**, *54*, 4349−4352.

(20) Miner, E. M.; Gul, S.; Ricke, N. D.; Pastor, E.; Yano, J.; Yachandra, V. K.; Van Voorhis, T.; Dincă, M. Mechanistic Evidence for Ligand−Centered Electrocatalytic Oxygen Reduction with the Conductive MOF Ni_3(hexaiminotriphenylene)$_2$. *ACS Catal.* **2017**, *7*, 7726−7731.
(21) Paz, F. A. A.; Klinowski, J.; Vilela, S. M. F.; Tomé, J. P. C.; Cavaleiro, J. A. S.; Rocha, J. Ligand design for functional metal-organic frameworks. *Chem. Soc. Rev.* **2012**, *41*, 1088−1110.
(22) Lu, W.; Wei, Z.; Gu, Z.-Y.; Liu, T.-F.; Park, J.; Park, J.; Tian, J.; Zhang, M.; Zhang, Q.; Gentle, T., III; Bosch, M.; Zhou, H.-C. Tuning the structure and function of metal-organic frameworks via linker design. *Chem. Soc. Rev.* **2014**, *43*, 5561−5593.
(23) D'Alessandro, D. M. Exploiting Redox Activity in Metal−Organic Frameworks: Concepts, Trends and Perspectives. *Chem. Commun.* **2016**, *52*, 8957−8971.
(24) Sun, L.; Hendon, C. H.; Minier, M. A.; Walsh, A.; Dincă, M. Million-Fold Electrical Conductivity Enhancement in Fe_2(DEBDC) versus Mn_2(DEBDC) (E = S, O). *J. Am. Chem. Soc.* **2015**, *137*, 6164−6167.
(25) Xie, L. S.; Sun, L.; Wan, R.; Park, S. S.; DeGayner, J. A.; Hendon, C. H.; Dincă, M. Tunable Mixed-Valence Doping toward Record Electrical Conductivity in a Three-Dimensional Metal-Organic Framework. *J. Am. Chem. Soc.* **2018**, *140*, 7411−7414.
(26) Gándara, F.; Uribe-Romo, F. J.; Britt, D. K.; Furukawa, H.; Lei, L.; Cheng, R.; Duan, X.; O'Keeffe, M.; Yaghi, O. M. Porous, Conductive Metal-Triazolates and Their Structural Elucidation by the Charge-Flipping Method. *Chem.—Eur. J.* **2012**, *18*, 10595−10601.
(27) Park, J. G.; Aubrey, M. L.; Oktawiec, J.; Chakarawet, K.; Darago, L. E.; Grandjean, F.; Long, G. J.; Long, J. R. Charge Delocalization and Bulk Electronic Conductivity in the Mixed-Valence Metal−Organic Framework Fe(1,2,3-triazolate)$_2$(BF_4)$_x$. *J. Am. Chem. Soc.* **2018**, *140*, 8526−8534.
(28) Pathak, A.; Shen, J.-W.; Usman, M.; Wei, L.-F.; Mendiratta, S.; Chang, Y.-S.; Sainbileg, B.; Ngue, C.-M.; Chen, R.-S.; Hayashi, M.; Luo, T.-T.; Chen, F.-R.; Tseng, T. W.; Chen, L.-C.; Lu, K.-L. Integration of a (−Cu−S−)n Plane in a Metal−Organic Framework Affords High Electrical Conductivity. *Nat. Commun.* **2019**, *10*, 1721.
(29) Takaishi, S.; Hosoda, M.; Kajiwara, T.; Miyasaka, H.; Yamashita, M.; Nakanishi, Y.; Kitagawa, Y.; Yamaguchi, K.; Kobayashi, A.; Kitagawa, H. Electroactive Porous Coordination Polymer Cu[Cu(pdt)$_2$] Composed of Donor and Acceptor Building Units. *Inorg. Chem.* **2009**, *48*, 9048−9050.
(30) Avendano, C.; Zhang, Z.; Ota, A.; Zhao, H.; Dunbar, K. R. Dramatically Different Conductivity Properties of Metal-Organic Framework Polymorphs of Tl(TCNQ): An Unexpected Room-Temperature Crystal-to-Crystal Phase Transition. *Angew. Chem., Int. Ed.* **2011**, *50*, 6543−6547.
(31) Fernandez, C. A.; Martin, P. C.; Schaef, T.; Bowden, M. E.; Thallapally, P. K.; Dang, L.; Xu, W.; Chen, X.; McGrail, B. P. An Electrically Switchable Metal-Organic Framework. *Sci. Rep.* **2015**, *4*, 6114.
(32) Darago, L. E.; Aubrey, M. L.; Yu, C. J.; Gonzalez, M. I.; Long, J. R. Electronic Conductivity, Ferrimagnetic Ordering, and Reductive Insertion Mediated by Organic Mixed-Valence in a Ferric Semiquinoid Metal-Organic Framework. *J. Am. Chem. Soc.* **2015**, *137*, 15703−15711.
(33) Ziebel, M. E.; Darago, L. E.; Long, J. R. Control of Electronic Structure and Conductivity in Two-Dimensional Metal-Semiquinoid Frameworks of Titanium, Vanadium, and Chromium. *J. Am. Chem. Soc.* **2018**, *140*, 3040−3051.
(34) Hmadeh, M.; Lu, Z.; Liu, Z.; Gándara, F.; Furukawa, H.; Wan, S.; Augustyn, V.; Chang, R.; Liao, L.; Zhou, F.; Perre, E.; Ozolins, V.; Suenaga, K.; Duan, X.; Dunn, B.; Yamamto, Y.; Terasaki, O.; Yaghi, O. M. New Porous Crystals of Extended Metal-Catecholates. *Chem. Mater.* **2012**, *24*, 3511−3513.
(35) Kambe, T.; Sakamoto, R.; Kusamoto, T.; Pal, T.; Fukui, N.; Hoshiko, K.; Shimojima, T.; Wang, Z.; Hirahara, T.; Ishizaka, K.; Hasegawa, S.; Liu, F.; Nishihara, H. Redox Control and High Conductivity of Nickel Bis(dithiolene) Complex π-Nanosheet: A Potential Organic Two-Dimensional Topological Insulator. *J. Am. Chem. Soc.* **2014**, *136*, 14357−14360.
(36) Sheberla, D.; Sun, L.; Blood-Forsythe, M. A.; Er, S.; Wade, C. R.; Brozek, C. K.; Aspuru-Guzik, A.; Dincă, M. High Electrical Conductivity in Ni_3(2,3,6,7,10,11-hexaiminotriphenylene)$_2$, a Semiconducting Metal−Organic Graphene Analogue. *J. Am. Chem. Soc.* **2014**, *136*, 8859−8862.
(37) Dou, J.-H.; Sun, L.; Ge, Y.; Li, W.; Hendon, C. H.; Li, J.; Gul, S.; Yano, J.; Stach, E. A.; Dincă, M. Signature of Metallic Behavior in the Metal−Organic Frameworks M_3(hexaiminobenzene)$_2$ (M= Ni, Cu). *J. Am. Chem. Soc.* **2017**, *139*, 13608−13611.
(38) Huang, X.; Sheng, P.; Tu, Z.; Zhang, F.; Wang, J.; Geng, H.; Zou, Y.; Di, C.; Yi, Y.; Sun, Y.; Xu, W.; Zhu, D. A Two-dimensional p−d Conjugated Coordination Polymer with Extremely High Electrical Conductivity and Ambipolar Transport Behavior. *Nat. Commun.* **2015**, *6*, 7408.
(39) Park, S. S.; Hontz, E. R.; Sun, L.; Hendon, C. H.; Walsh, A.; Van Voorhis, T.; Dincă, M. Cation-Dependent Intrinsic Electrical Conductivity in Isostructural Tetrathiafulvalene-Based Microporous Metal-Organic Frameworks. *J. Am. Chem. Soc.* **2015**, *137*, 1774−1777.
(40) Xie, L. S.; Alexandrov, E. V.; Skorupskii, G.; Proserpio, D. M.; Dincă, M. Diverse π-π stacking motifs modulate electrical conductivity in tetrathiafulvalene-based metal-organic frameworks. *Chem. Sci.* **2019**, *10*, 8558−8565.
(41) Skorupskii, G.; Trump, B. A.; Kasel, T. W.; Brown, C. M.; Hendon, C. H.; Dincă, M. Efficient and tunable one-dimensional charge transport in layered lanthanide metal-organic frameworks. *Nat. Chem.* **2020**, *12*, 131−136.
(42) Kuang, X.; Chen, S.; Meng, L.; Chen, J.; Wu, X.; Zhang, G.; Zhong, G.; Hu, T.; Li, Y.; Lu, C.-Z. Supramolecular Aggregation of a Redox-Active Copper-Naphthalenediimide Network with Intrinsic Electron Conduction. *Chem. Commun.* **2019**, *55*, 1643−1646.
(43) Chen, D.; Xing, H.; Su, Z.; Wang, C. Electrical conductivity and electroluminescence of a new anthracene-based metal-organic framework with π-conjugated zigzag chains. *Chem. Commun.* **2016**, *52*, 2019−2022.
(44) Zeng, M.-H.; Wang, Q.-X.; Tan, Y.-X.; Hu, S.; Zhao, H.-X.; Long, L.-S.; Kurmoo, M. Rigid Pillars and Double Walls in a Porous Metal-Organic Framework: Single-Crystal to Single-Crystal, Controlled Uptake and Release of Iodine and Electrical Conductivity. *J. Am. Chem. Soc.* **2010**, *132*, 2561−2563.
(45) Kobayashi, Y.; Jacobs, B.; Allendorf, M. D.; Long, J. R. Conductivity, Doping, and Redox Chemistry of a Microporous Dithiolene-Based Metal−Organic Framework. *Chem. Mater.* **2010**, *22*, 4120−4122.
(46) Talin, A. A.; Centrone, A.; Ford, A. C.; Foster, M. E.; Stavila, V.; Haney, P.; Kinney, R. A.; Szalai, V.; El Gabaly, F.; Yoon, H. P.; Léonard, F.; Allendorf, M. D. Tunable Electrical Conductivity in Metal-Organic Framework Thin-Film Devices. *Science* **2014**, *343*, 66−69.
(47) Guo, Z.; Panda, D. K.; Maity, K.; Lindsey, D.; Parker, T. G.; Albrecht-Schmitt, T. E.; Barreda-Esparza, J. L.; Xiong, P.; Zhou, W.; Saha, S. Modulating the electrical conductivity of metal-organic framework films with intercalated guest π-systems. *J. Mater. Chem. C* **2016**, *4*, 894−899.
(48) Guo, Z.; Panda, D. K.; Gordillo, M. A.; Khatun, A.; Wu, H.; Zhou, W.; Saha, S. Lowering Band Gap of an Electroactive Metal-Organic Framework via Complementary Guest Intercalation. *ACS Appl. Mater. Interfaces* **2017**, *9*, 32413−32417.
(49) Wang, H.-Y.; Ge, J.-Y.; Hua, C.; Jiao, C.-Q.; Wu, Y.; Leong, C. F.; D'Alessandro, D. M.; Liu, T.; Zuo, J.-L. Photo- and Electronically Switchable Spin-Crossover Iron(II) Metal-Organic Frameworks Based on a Tetrathiafulvalene Ligand. *Angew. Chem., Int. Ed.* **2017**, *56*, 5465−5470.
(50) Su, J.; Yuan, S.; Wang, H.-Y.; Huang, L.; Ge, J.-Y.; Joseph, E.; Qin, J.; Cagin, T.; Zuo, J.-L.; Zhou, H.-C. Redox-Switchable Breathing Behavior in Tetrathiafulvalene-Based Metal−Organic Frameworks. *Nat. Commun.* **2017**, *8*, 2008−2016.

https://dx.doi.org/10.1021/acsami.0c12388
ACS Appl. Mater. Interfaces XXXX, XXX, XXX−XXX

(51) Gordillo, M. A.; Benavides, P. A.; Panda, D. K.; Saha, S. The Advent of Electrically Conducting Double-Helical Metal-Organic Frameworks Featuring Butterfly-Shaped Electron-Rich π-Extended Tetrathiafulvalene Ligands. *ACS Appl. Mater. Interfaces* **2020**, *12*, 12955−12961.
(52) Goswami, S.; Ray, D.; Otake, K.-i.; Kung, C.-W.; Garibay, S. J.; Islamoglu, T.; Atilgan, A.; Cui, Y.; Cramer, C. J.; Farha, O. K.; Hupp, J. T. A porous, electrically conductive hexa-zirconium(iv) metal-organic framework. *Chem. Sci.* **2018**, *9*, 4477−4482.
(53) Goswami, S.; Hod, I.; Duan, J. D.; Kung, C.-W.; Rimoldi, M.; Malliakas, C. D.; Palmer, R. H.; Farha, O. K.; Hupp, J. T. Anisotropic Redox Conductivity within a Metal-Organic Framework Material. *J. Am. Chem. Soc.* **2019**, *141*, 17696−17702.
(54) Wentz, H. C.; Skorupskii, G.; Bonfim, A. B.; Mancuso, J. L.; Hendon, C. H.; Oriel, E. H.; Sazama, G. T.; Campbell, M. G. Switchable electrical conductivity in a three-dimensional metal-organic framework via reversible ligand n-doping. *Chem. Sci.* **2020**, *11*, 1342−1346.
(55) Zheng, S.-L.; Zhang, J.-P.; Wong, W.-T.; Chen, X.-M. A Novel, Highly Electrical Conducting, Single-Component Molecular Material: $[Ag_2(ophen)_2]$ (Hophen = 1H-[1,10]phenanthrolin-2-one). *J. Am. Chem. Soc.* **2003**, *125*, 6882−6883.
(56) Szalay, P. S.; Galán-Mascarós, J. R.; Clérac, R.; Dunbar, K. R. $HAT(CN)_6$: A New Building Block for Molecule-Based Magnetic Materials. *Synth. Met.* **2001**, *122*, 535−542.
(57) Okubo, T.; Kitagawa, S.; Kondo, M.; Matsuzaka, H.; Ishii, T. A New Anion-Trapping Radical Host, $[(Cu\text{-}dppe)_3\{hat\text{-}(CN)_6\}]^{2+}$. *Angew. Chem., Int. Ed.* **1999**, *38*, 931−933.
(58) Furukawa, S.; Okubo, T.; Masaoka, S.; Tanaka, D.; Chang, H.-C.; Kitagawa, S. Effect of the Metal-Assisted Assembling Mode on the Redox States of Hexaazatriphenylene Hexacarbonitrile. *Angew. Chem., Int. Ed.* **2005**, *44*, 2700−2704.
(59) Kitagawa, S.; Masaoka, S. Metal complexes of hexaazatriphenylene (hat) and its derivatives-from oligonuclear complexes to coordination polymers. *Coord. Chem. Rev.* **2003**, *246*, 73−88.
(60) Chifotides, H. T.; Schottel, B. L.; Dunbar, K. R. The π-Accepting Arene $HAT(CN)_6$ as a Halide Receptor through Charge Transfer: Multisite Anion Interactions and Self-Assembly in Solution and the Solid State. *Angew. Chem., Int. Ed.* **2010**, *49*, 7202−7207.
(61) Aragay, G.; Frontera, A.; Lloveras, V.; Vidal-Gancedo, J.; Ballester, P. Different Nature of the Interactions Between Anions and $HAT(CN)_6$: From Reversible Anion−π Complexes to Irreversible Electron-Transfer Processes ($HAT(CN)_6$ = 1,4,5,8,9,12-Hexaazatriphenylene). *J. Am. Chem. Soc.* **2013**, *135*, 2620−2627.
(62) Kobylarczyk, J.; Pinkowicz, D.; Srebro-Hooper, M.; Hooper, J.; Podgajny, R. Anion−π recognition between $[M(CN)_6]^{3-}$ complexes and $HAT(CN)_6$]: structural matching and electronic charge density modification. *Dalton Trans.* **2017**, *46*, 3482−3491.
(63) Kuzniak, E.; Pinkowicz, D.; Hooper, J.; Srebro-Hooper, M.; Hetmańczyk, Ł.; Podgajny, R. Molecular Deformation, Charge Flow, and Sponge-like Behavior in Anion−π $\{[M(CN)_4]^{2-};[HAT(CN)_6]\}_\infty$ (M= Ni, Pd, Pt) Supramolecular Stacks. *Chem.—Eur. J.* **2018**, *24*, 16302−16314.
(64) Kobylarczyk, J.; Pinkowicz, D.; Srebro-Hooper, M.; Hooper, J.; Podgajny, R. Anion−π Architectures of $HAT(CN)_6$] and 5d Polycyanidometalates: $[W(CN)_8]^{3-}$, $[Re(CN)_7]^{3-}$ and $[Pt(CN)_6]^{2-}$. *Cryst. Growth Des.* **2019**, *19*, 1215−1225.
(65) Saha, S. Anion-Induced Electron Transfer. *Acc. Chem. Res.* **2018**, *51*, 2225−2236.
(66) Schottel, B. L.; Chifotides, H. T.; Dunbar, K. R. Anion-π interactions. *Chem. Soc. Rev.* **2008**, *37*, 68−83.
(67) Liao, L. S.; Slusarek, W. K.; Hatwar, T. K.; Ricks, M. L.; Comfort, D. L. Tandem Organic Light-Emitting Diode using Hexaazatriphenylene Hexacarbonitrile in the Intermediate Connector. *Adv. Mater.* **2008**, *20*, 324−329.
(68) Kim, S. Y.; Jeon, W. S.; Park, T. J.; Pode, R.; Jang, J.; Kwon, J. H. Low Voltage Efficient Simple p-i-n Type Electrophosphorescent Green Organic Light-Emitting Devices. *Appl. Phys. Lett.* **2009**, *94*, 133303.
(69) Dai, Y.; Zhang, H.; Zhang, Z.; Liu, Y.; Chen, J.; Ma, D. Highly efficient and stable tandem organic light-emitting devices based on HAT-CN/HAT-CN:TAPC/TAPC as a charge generation layer. *J. Mater. Chem. C* **2015**, *3*, 6809−6814.
(70) Rademacher, J. T.; Kanakarajan, K.; Czarnik, A. W. Improved Synthesis of 1,4,5,8,9,12-Hexaazatriphenylenehexacarboxylic acid. *Synthesis* **1994**, 378−380.

https://dx.doi.org/10.1021/acsami.0c12388
ACS Appl. Mater. Interfaces XXXX, XXX, XXX−XXX